We are IntechOpen, the world's leading publisher of Open Access books Built by scientists, for scientists

4,800
Open access books available

122,000
International authors and editors

135M
Downloads

Our authors are among the

154
Countries delivered to

TOP 1%
most cited scientists

12.2%
Contributors from top 500 universities

CLARIVATE ANALYTICS BOOK CITATION INDEX INDEXED

WEB OF SCIENCE™

Selection of our books indexed in the Book Citation Index in Web of Science™ Core Collection (BKCI)

Interested in publishing with us?
Contact book.department@intechopen.com

Numbers displayed above are based on latest data collected.
For more information visit www.intechopen.com

3

Tailoring the Interface Properties of Magnetite for Spintronics

Gareth S. Parkinson[1], Ulrike Diebold[1], Jinke Tang[2] and Leszek Malkinski[3]
[1]*Institute of Applied Physics, Vienna University of Technology, Vienna,*
[2]*Department of Physics and Astronomy, University of Wyoming, Laramie, WY*
[3]*Advanced Materials Research Institute and the Department of Physics, University of New Orleans, Lakeshore Dr., New Orleans, LA*
[1]*Austria*
[2,3]*USA*

1. Introduction

1.1 Spintronics and spintronic materials

The field of spintronics originates from the discovery of giant magnetoresistance (GMR) by Fert and Grünberg [1, 2] in 1988, for which they were awarded Nobel Prize in 2007. This effect, first observed in nanostructures comprised of two thin magnetic layers of Fe separated by a 1-2 nm thick Cr spacer, was both qualitatively and quantitatively different from the prior-known phenomenon of anisotropic magnetoresistance. GMR leads to magnetoresistance much larger than anisotropic magnetoresistance. Given the exciting nature of the effect, the underlying mechanism was promptly investigated and quickly understood [3]. Essentially, GMR can be described in terms of spin filtering; conduction electrons are polarized in one ferromagnetic layer, maintain spin memory while traveling through a thin spacer, and then enter the second magnetic layer. The scattering of electrons in this second magnetic layer depends on the direction of the magnetization relative to the first (polarizing) layer. The electrons pass through the two layers almost unperturbed if their respective magnetization is parallel. In contrast they experience enhanced scattering for an antiparallel magnetization configuration. This magnetization-dependent scattering potential can be explained through the availability (or non availability) of electron states in the second material around the Fermi level in the spin-up and spin down bands. Consequently, spintronics relies on materials in which a spin asymmetry exists in the density of states at the Fermi level. Such differences down in magnetically ordered materials arise from exchange interactions between magnetic atoms. The extreme case of energy band splitting occurs in half metals, where only one spin orientation can be occupied by electrons at the Fermi level. Therefore, half-metals should behave as a conductor for the electron current when electron spins match the direction of magnetization and as an insulator when the spin direction opposes the magnetization.

While the first observations of GMR were made in the Fe/Cr system of antiferromagnetically coupled Fe layers forming tri-layer spin valve structures or multilayers, it was quickly realized that the Ruderman-Kittel-Kasuya-Yosida (RKKY) type interaction between the Fe layers through the Cr spacer, responsible for this coupling, was not a necessary condition for the occurrence of the GMR effect. What really matters is that the antiparallel alignment of the magnetization in the magnetic layers in some range of the applied magnetic field. This effect could be achieved either using dissimilar magnetic layers (e.g. different thickness of the films or different materials constituting the layers) or by pinning the magnetization of the one of the layers using exchange interaction. This can be realized using a magnetically harder ferromagnetic or antiferromagnetic material, such that switching of the free layer occurs prior to the pinned (or harder) layer. One of the disadvantages of the antiferromagnetic coupling was the oscillation of its strength and sign (change from anti- to ferromagnetic) with thickness of the spacer layer, which limited the spacer thickness to 2 nm and imposed tough requirements on the technology. A new mechanism of switching the magnetization in the layers enabled the discovery that the spin diffusion length could be greater than just 2 nm, and allowed the building of structures with 4 to 6 nm spacer layers with performance nearly independent of fluctuations in the spacer thickness. A variety of materials have been tested and GMR, defined as MR = $(R_{max}-R_{min})/R_{min}$ (were R_{min} and R_{max} denote minimum and maximum resistance of the sample) exceeding 100% has been observed in the Co/Cu multilayers [4]. Shortly after the discovery of GMR it was demonstrated that this effect is not unique to layered structures, and significant magnetoresistance values were measured in granular systems of Co nanoparticles embedded in a Cu matrix [5].

The success of giant magnetoresistive structures encouraged researchers to study similar structures comprising two magnetic layers separated by an insulating barrier. Such architectures are similar to those in which Julliere discovered magnetoresistance at low temperatures back in 1975 [6]. It took Miyazaki [7] and Moodera [8] to realize that these structures can easily compete with the GMR structures. Transition metals with a 1 nm thick barrier of aluminum oxide or titanium oxide display a 40 to 80 % relative change of the resistance, exceeding the performance of spin-valves (of about 15%) by a factor of 5. Many of the critical features defining the magnetoersistance in tunneling junctions, or the tunneling magnetoresistance (TMR), remain similar to those important for GMR. The key difference of course, is that the electrons now tunnel from one material to another magnetic material through a barrier, replacing ballistic conduction.

The potential for using the GMR effect in magnetic field sensors and hard drive read heads was quickly recognized by companies in the information technology sector. Dynamic progress in research on GMR and TMR effects laid the foundations of a new discipline in electronics initiated by the publication of Prinz [9] in 1998, who suggested that spin dependent transport does not have to be limited to analog magnetic sensors, but can be developed into a branch of electronics that takes full advantage of electron spin. The name given to the emerging discipline evolved from magnetoelectronics, spin electronics and, finally, to spintronics, describing a new generation of nonvolatile electronic devices which use magnetization of spin valve structures to store or process digital information. More details can be found in several books and review articles on spintronics [10-12]

Current magnetoresistive devices such as magnetoresistive random access memories are based on transition metals and their alloys. The excellent performance of tunneling junctions with an MgO barrier, demonstrated by Yuasa [13] and Parkin [14] approached the theoretical limit of TMR for the transition metal based junctions. In order to compete with semiconducting switches and transistors, which change resistance by more than 6 orders of magnitude, the relative changes of resistance of spintronic devices must be improved by a few orders of magnitude. The only option to achieve this goal is to search for new magnetic materials that exhibit a higher degree of spin polarization than transition metals. While some researchers explore magnetic semiconductors as potential candidates for spintronic devices, half-metallic materials provide an attractive alternative path toward the challenging goal of further improving the performance of spintronic devices.

In addition to the more complex Heusler alloys, the binary compounds CrO_2 and Fe_3O_4 (magnetite) are primary half metal candidates for spintronic applications [15]. While spectroscopy measurements demonstrated 98.4% spin polarization of CrO_2 [16, 17], its performance in spintronic materials and devices has been rather disappointing. For the last decade many researchers have tried to understand this discrepancy and have attempted to improve the properties of the spintronic properties of CrO_2 based devices [18-31]. A similar problem has been found in Fe_3O_4–based structures, which have underperformed compared to expectations. In both cases, a reduction in the magnetoresistance has been attributed to surface modifications of these oxides occurring at the interfaces. Here, we will discuss how the surface properties of single crystal magnetite, particularly those of the (001) surface reconstruction, can produce an environment detrimental to the transport of a spin polarized current. Further, we discuss the possibility to preserve the half metallic character of this magnetic oxide on the surface of single crystals and nanoparticles by surface engineering. Our results show that molecular adsorption has a strong effect on the electronic structure of the interface, evidenced by spectroscopy results and enhanced magnetoresistance.

2. Structure and properties of Fe_3O_4

Spintronic devices, rely on materials in which a spin asymmetry can be established at the Fermi level, allowing the on/off state of a device to be controlled through the manipulation of a spin dependent charge transfer mechanism. An example of the principle of operation of a simple spintronic device, magnetic tunnel junction, where magnetic fields or spin current torques are used to switch the alignment of two ferromagnetic electrodes between a parallel and anti-parallel condition is illustrated in Fig. 1. With the spins aligned, a spin-polarized current can flow through the device as there are corresponding states available at the Fermi level. In contrast, with antiparallel alignment, there are no matching states at the Fermi level into which spin polarized electrons can flow and the device is in the off state. In the ideal device, the magneto resistance, i.e., the difference in resistance between the on and off states, is maximized. In recent years there has been much research into suitable materials with which to realize the spintronics dream, but it is clear that the optimum electrode materials should possess 100% spin polarization at the Fermi level, since this ensures that zero current flows in the “off” state.

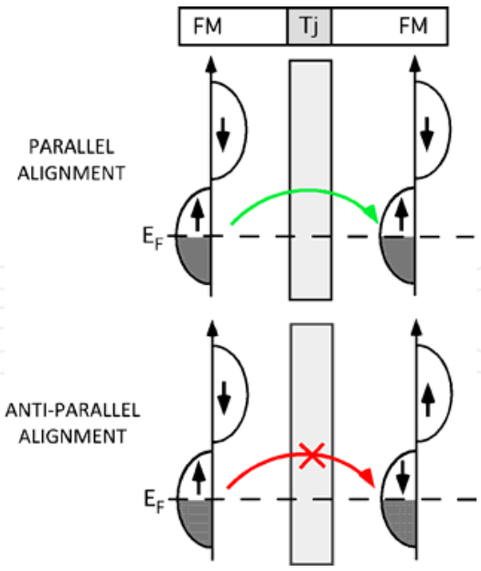

Fig. 1. Schematic of a magnetic tunnel junction. (top) Parallel alignment of two magnetic electrodes leads to tunneling of up-spin electrons through the insulating tunnel junction (Tj). (bottom) Anti-parallel alignment leads to high resistance since there are no matching states available at E_F

The considerations described above led to a surge of interest in half-metallic ferromagnets, including Fe_3O_4, which exhibits nearly 100% spin polarization at the Fermi level [32-35]. However in magnetite, which is particularly attractive to industry due to its ubiquity and inexpensive production, the expected benefits of 100% spin polarization have never been realized in prototype devices [36-41]. In fact, the highest magnetoresistance reported to date for a Fe_3O_4 based device is a mere 16 %. This disappointing turn of events is more often than not attributed to interface effects [42-45]. More specifically, it is thought that the problem lies in efficiently injecting the spin polarized current from a Fe_3O_4 electrode into a semiconductor. Unfortunately, the interface between Fe_3O_4 and a semiconducting buffer layer represents the most ill-defined region of such a device, and little is known about the factors that govern the electronic properties of the interface. This has led to a somewhat ad-hoc approach to performance improvement, i.e., constructing device prototypes using a variety of semiconductors and then measuring the resulting magnetoresistance and explaining the results afterwards.

In this section we discuss the alternative approach toward improving the performance of Fe_3O_4 based spintronics devices i.e. developing an understanding of the fundamental processes governing Fe_3O_4-semiconductor interface properties, and then using this knowledge to deterministically tailor suitable interfaces for certain tasks. More specifically, we describe recent progress toward understanding the properties of Fe_3O_4 through atomic scale studies of its' (001) surface, and how early experiments show that the surface properties can be affected by adsorbates. It is demonstrated herein that the electronic properties of the clean Fe_3O_4(001) surface diverge strongly from those of the bulk material as a result of a subtle surface reconstruction. Further, we demonstrate that surface engineering through adsorption represents a valid route toward tailoring the electronic structure, and consequently the spin transport properties at spintronic interfaces.

Fe_3O_4 crystallizes in the inverse spinel structure, which comprises a cubic close packed oxygen lattice with Fe cations occupying interstitial sites [46]. In the inverse spinel structure Fe^{3+} cations occupy 1/8 of the tetrahedral interstitial "A" sites and a 50:50 mixture of Fe^{3+} and Fe^{2+} cations occupy 1/2 of the octahedral "B" sites. The differing and opposed magnetic moment on the A and B sublattices results in ferrimagnetism (T_C = 858 K) with a magnetic moment of $4\mu_B$ per unit cell. In 1939, Verwey discovered a metal-insulator transition in Fe_3O_4 (T_V =123 K) [47,48] in which the conductivity drops by two orders of magnitude on cooling. Coincident with the electronic changes, the crystal structure goes from cubic to monoclinic. For the room temperature conductive phase, Verwey proposed that the conduction mechanism was electron hopping between Fe^{2+} and Fe^{3+} cations on the B sublattice [47,48]. However despite several decades of intense research, the conduction mechanism remains a controversial topic in the literature. Recent experiments have shown measured little difference in the charge between Fe(B) atoms, and today the charge is commonly written as $Fe^{2.5+}$ to reflect the extent of electron delocalization [48]. This makes Fe_3O_4 a particularly challenging system for modern theoretical calculations.

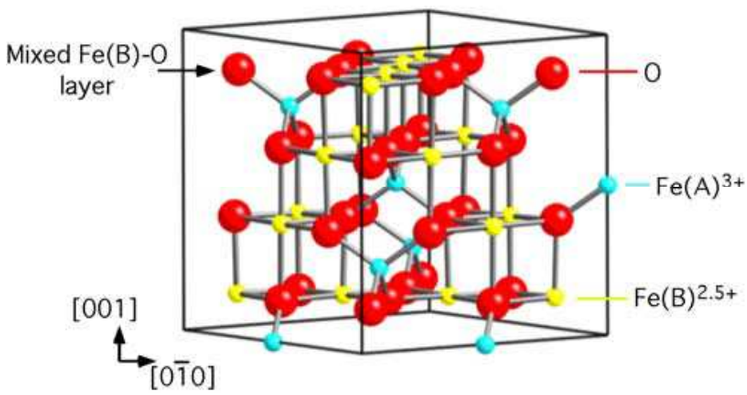

Fig. 2. Fe_3O_4 bulk unit cell (inverse spinel structure)

The interest in using Fe_3O_4 in spintronic applications arose in the 1980's, when band structure calculations predicted that the room temperature phase is half-metallic [49,50], with only minority spin electrons responsible for the conduction. This occurs because the 5-fold degenerate d levels of the Fe(B) cations are split by the crystal field into 3 t_{2g} orbitals and 2 e_g orbitals. For both the Fe^{3+} and Fe^{2+} cations the spin up levels are occupied. However, for the Fe^{2+} cations, the extra electron occupies the lowest lying t_{2g} orbital of the spin down state (marked by a gray arrow in Figure 3), which sits at the Fermi level. While this result has been confirmed by other theoretical calculations, experimental verification of this exciting prediction has not been forthcoming, despite significant effort.

The most common method for the absolute measurement of spin polarization, Andreev reflection [51], requires measurements at extremely low temperatures. Unfortunately this is not possible for the conducting phase of Fe_3O_4 as the Verwey transition occurs at 123 K [47,48]. Consequently, alternative methods to measure the Fermi level spin polarization were sought. Several groups performed spin resolved photoemission spectroscopy [52] (SP-PES)

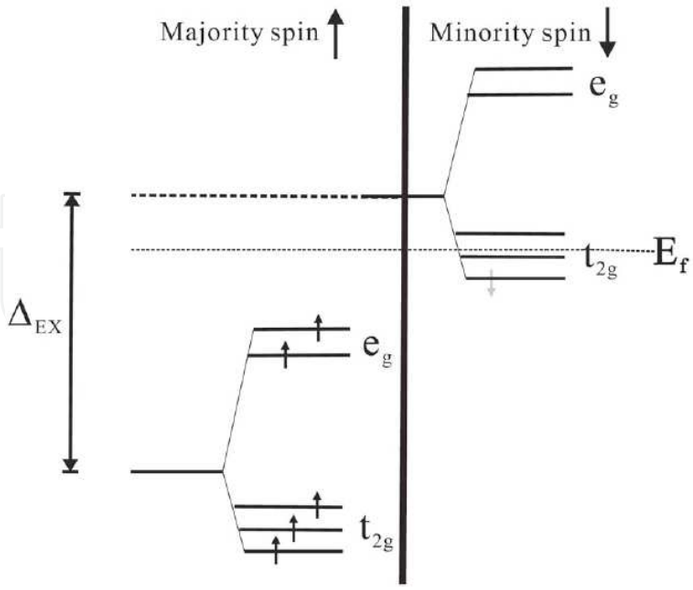

Fig. 3. Schematic representation of the energy levels on the Fe(B) sublattice in Fe_3O_4. Only down spin electrons are present at the Fermi level. Figure reproduced from ref. 33

experiments, where UV light excites photo-electrons directly from the valence band, which are analyzed by a spin sensitive electron analyzer. By including spin sensitive Mott detector [52], the fraction of spin-up and spin-down electrons at the Fermi level can be calculated. However, the measured values of the spin polarization in Fe_3O_4 vary wildly from group to group, and from sample to sample, with reported values ranging from 20-80% [53-56]. Thus, for several years there has been confusion and debate regarding the real spin polarization of Fe_3O_4.

In the light of the experimental results to be described in this chapter, it appears that the primary issue affecting the SP-PES measurements is that photoemission is an inherently surface sensitive technique. Since the mean free path of low energy electrons is extremely short in solids, the measured electrons emerge only from the first few atomic layers of the sample. Consequently, photoemission can only be reliably used to measure bulk properties if the surface layers are representative of bulk properties. If a material exhibits strong surface effects, the measurements reflect a superposition of the bulk and surface. In this regard, recent work has shown that Fe_3O_4 *does not* form simple bulk-truncated surfaces, and that Fe_3O_4 surface properties deviate dramatically from those of the bulk. While the inability to extract spin-polarized electrons from Fe_3O_4 surfaces provides a satisfactory explanation of the erroneous SP-PES results, it also provides a rationale for understanding the poor performance of Fe_3O_4 based spintronic devices.

3. Fe_3O_4 surfaces

The most energetically favorable Fe_3O_4 surfaces are the (111) and (001) planes. In recent years the surface science method, where single crystal samples are studied in a highly

controlled UHV environment, has been applied to characterize these surfaces and the most common terminations have been determined. At the Fe_3O_4(111) surface, three distinct terminations are possible, exposing either O, Fe(B) or Fe(A) atoms [57]. However, often the different terminations are found to coexist on the surface, with their relative coverage strongly dependent on the oxidation conditions during sample preparation [57]. This makes quantitative analysis of the surface properties problematic and difficult to reproduce exactly.

In contrast, it is now well established that the energetically favorable termination of the (001) surface is a mixed Fe(B)-O layer across a wide range of O chemical potentials [34,58-61]. However, low energy electron diffraction (LEED) patterns exhibit a (√2×√2)R45° symmetry, indicative of surface reconstruction (see fig. 4.a, the black square indicates the (√2×√2)R45° unit cell). The generally accepted structural model for this surface was proposed on the basis of a combined experiment-theory study in 2005 [58]. Essentially, the surface undergoes a Peierls-like distortion, in which a small amount of energy is saved by doubling the periodicity along the surface Fe(B) rows (see fig. 4.b,c). This model is consistent with STM images (fig. 5) [32, 62,63], which show alternate pairs of Fe(B) atoms relaxing in opposite directions perpendicular to the Fe(B) row direction. As neighboring rows relax in antiphase to one another, the (√2×√2)R45° surface unit cell is produced, as indicated by the cyan square in figure 5.

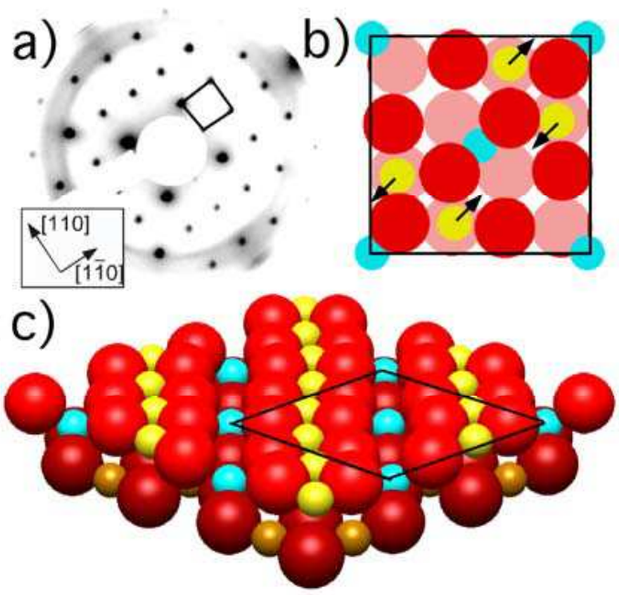

Fig. 4. a) LEED pattern recorded for 90 eV electron energy. (b) Fe_3O_4(001) surface unit cell (c) perspective view of Fe_3O_4(001) in which the undulations of the surface reconstruction are visible. Figure adapted from ref. 32

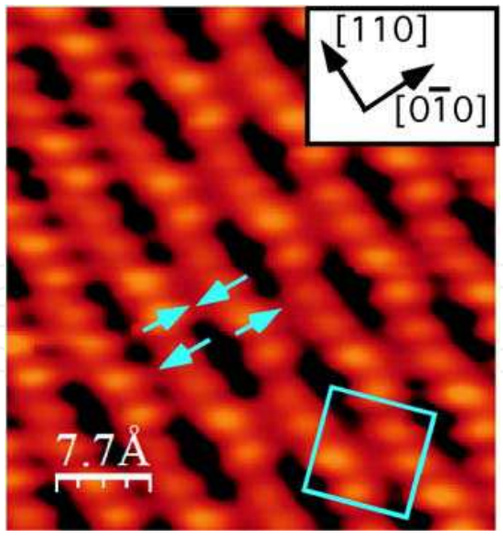

Fig. 5. 4x4 nm² STM image of the Fe_3O_4(001) surface (V_{SAMPLE}=1.2 V, I_{TUNNEL}=0.3 nA). Adapted from Ref. 32

Further DFT calculations of the Fe_3O_4(001) surface soon followed, extending on their predecessors by including a Hubbard "U" parameter to take account of electron correlation, which is significant in Fe_3O_4 [34,59]. These calculations reveal that charge order in the subsurface layers couples to the lattice distortion, resulting in the shift of the t_{2g} orbitals above the Fermi level, and the opening of a small bandgap in the surface layers. The surface band gap was experimentally measured at 0.2 eV in scanning tunneling spectroscopy experiments [33] (see figure 6b). These results taken together provide ample evidence that Fe_3O_4 is a material exhibiting strong surface effects. From this viewpoint, it is possible to

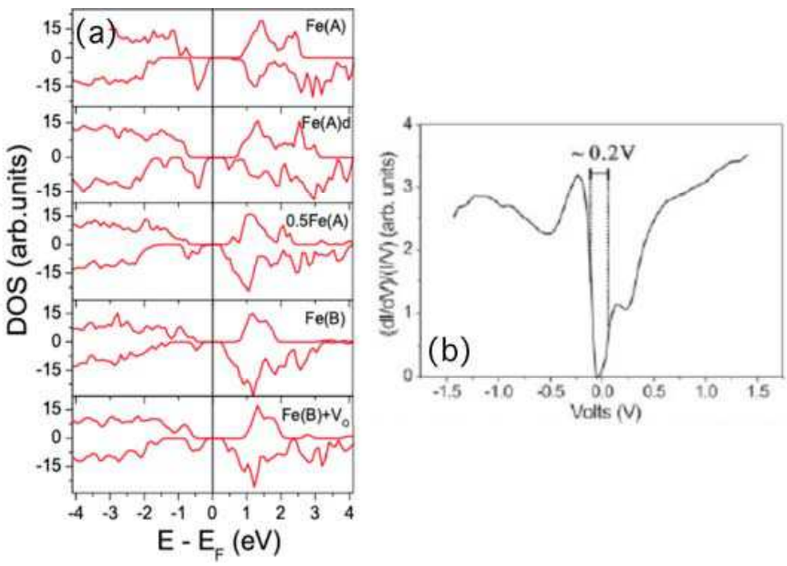

Fig. 6. DOS calculations for the Fe_3O_4(001) surface which show that a surface band gap exists irrespective of the surface termination model. Reproduced from ref. 34 (b) STS results which demonstrate a band gap of 0.2 eV at the Fe_3O_4(001) surface. Reproduced from ref. 33

explain the erroneous spin polarization measurements described above, and to rationalize the poor performance of Fe_3O_4 based spintronics devices.

The Fe_3O_4(001) surface represents one of the best characterized examples of the effect of surface reconstruction on electronic properties. Consequently, this system provides a perfect testing ground for experiments into the possibility of utilizing surface engineering to try and recover the bulk transport properties in the surface. Since the primary characteristic that distinguishes a surface from the bulk is the under coordination of surface atoms compared to their bulk counterparts, it is plausible that the addition of new bonds through the adsorption of molecules could modify the surface properties.

4. Fe_3O_4(001)–H – Recovery of surface half-metalicity

The simplest possible adsorbate that one can add to a metal-oxide surface is a single H atom. Atomic H has the advantage of being both computationally tractable and relatively simple to deposit cleanly in ultra-high vacuum experiments. Essentially, one simply backfills the vacuum system with a partial pressure of H_2 (~ 10^{-6} mbar) and then dissociates molecules close to the sample surface using a hot W filament. A fraction of the reactive atomic H are then directly incident to the sample surface, where they stick with unit probability. By changing the H_2 pressure and/or the exposure time it is possible to systematically vary the sample exposure.

The natural adsorption site for H atoms on a metal-oxide surface is the surface O atom, leading to the formation of surface hydroxyl groups. This expectation is confirmed by peaks associated with surface hydroxyl groups visible in both valence band (UPS) and core level (XPS) photoemission measurements upon saturation atomic H deposition (XPS data not shown).

However, the most interesting photoemission data occurs at the Fermi level (inset, figure 7a), where a huge increase in the density of states is observed, i.e. a metallization of the surface. Clearly, this result shows that adsorption is capable of inducing massive changes to the electronic structure at Fe_3O_4 surfaces. Independent but complementary measurements of the same system using a spin sensitive probe (metastable He-scattering) have shown that the

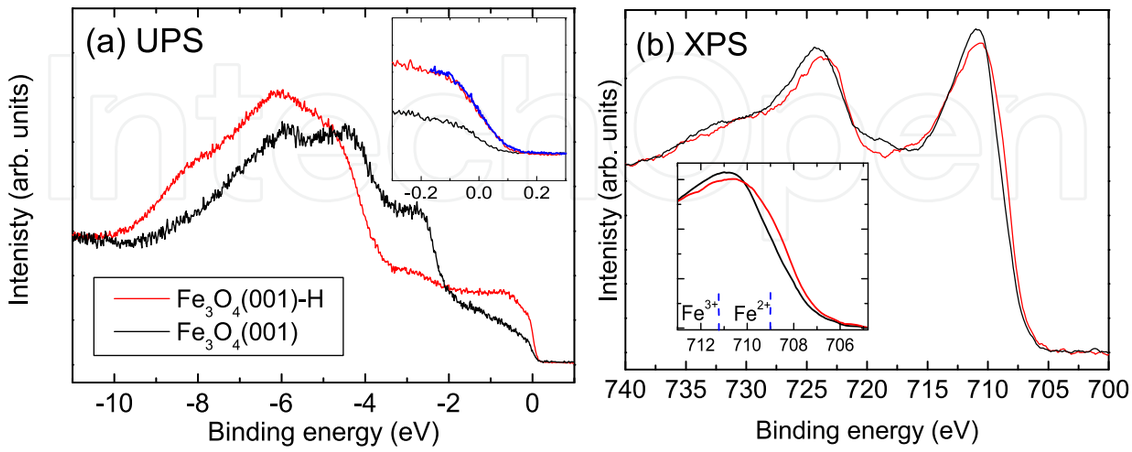

Fig. 7. (a) UPS spectra of the Fe_3O_4(001) valance band before and after saturation atomic H adsorption. (b) XPS spectra for the Fe *2p* core levels before and after atomic H exposure. Figure reproduced from ref. 32

H-induced density of states at the Fermi level are highly spin polarized (> 50 %) [64], exactly the result required for spintronic applications.

5. Fe_3O_4(001)-H – Mechanism

While the possibility to remove the Fe_3O_4(001) surface bandgap via atomic H adsorption is an important discovery, it is crucial that we understand the fundamental processes that underlie the macroscopic electronic changes. This is particularly important for the case of the H-Fe_3O_4(001) system because it is highly unlikely that a monolayer (ML) of H atoms could be stabilized in a device architecture. Therefore, one needs to understand as much as possible about the mechanism responsible for the half-metallization in order to be able to reproduce the effect with other, more technologically relevant adsorbates.

To this end we investigated the adsorption of atomic H on the Fe_3O_4(001) surface using several complementary surface science techniques. Firstly, the XPS measurements presented in figure 7b show a significant shift in the Fe *2p* peaks toward lower binding energy, consistent with a change in the valance of the surface Fe atoms from Fe^{3+} to Fe^{2+} character. This suggests that the atomic H has a significant impact on the properties of the surface Fe cations, despite the fact that it bonds directly only to the oxygen atoms. This is very important since conduction is thought to occur on the Fe(B) sublattice.

Typically, the first technique applied in a surface science experiment aimed at investigating structure is low energy electron diffraction. This technique provides instant qualitative information regarding changes in the surface symmetry and an assessment of the quality of the surface order can be made. Monitoring the Fe_3O_4(001) LEED pattern as a function of exposure, it was observed that the diffraction spots related to the surface reconstruction fade and eventually disappear at the highest exposures, resulting in a (1×1) LEED pattern (see figure 8b). This suggests that the surface reconstruction is lifted by atomic H adsorption, and therefore that the surface may be representative of the Fe_3O_4(001) bulk.

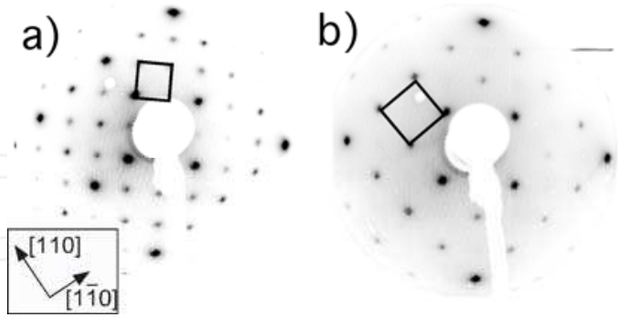

Fig. 8. Fe_3O_4(001) LEED pattern before (a) and after (b) saturation atomic H exposure. The symmetry changes from (√2×√2)R45° to (1×1). Figure adapted from Ref. 32

To extend upon the LEED analysis we utilized scanning tunneling microscopy (STM) [65] to investigate atomic H adsorption at the atomic scale. In an STM experiment, an atomically sharp STM tip (typically W) is brought very close to a sample surface, close enough that electrons can tunnel between them. With the application of a sample bias (of the order 1 V), a measurable current (of the order 1 nA) is observed. Scanning the tip across the surface and utilizing a feedback loop to keep the tunneling current constant, a topographical image of

the surface can be constructed. It is important to note that the image is not a direct measure of the surface topography alone, rather it is effectively a contour plot of the surface electronic density of states. This results, for example, in the low lying Ti atoms being imaged brighter than the protruding O atoms in images of the TiO_2(110) surface [66,67].

In the STM images of the hydroxylated Fe_3O_4(001) surface (fig. 9), a similar case of electronic contrast is observed. The H atoms bound to the surface O are not directly observed, but their presence leads to a change in the density of states at the neighboring Fe(B) atom pair, resulting in an enhancement of their contrast in STM. When the H atom jumps the small distance to the symmetrically equivalent O atom within the unit cell, the electronic effect is transferred to the opposite Fe(B) row. This back and forth diffusion between the two sites is observed frequently at room temperature in STM movies (i.e. series of images collected on the same sample area). Two frames from such a movie are shown as figure 9a,b.

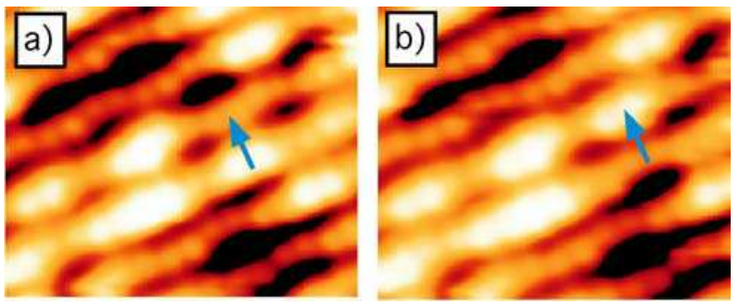

Fig. 9. Sequential STM images of the Fe_3O_4 following atomic H exposure (4x3.5 nm^2, V_{SAMPLE}=1.2 V, I_{TUNNEL}=0.3 nA). Between the two images one bright pair jumps to the opposite Fe(B) row (indicated by the blue arrow). Adapted from Ref. 32

From these STM images it is also possible to discern that atomic H has a strong preference for bonding to one particular O atom site within the surface unit cell; where the Fe(B) rows relax towards each other, hereafter called the O_{NARROW} site (see fig. 10 for a schematic model). The observed preference for the O_{NARROW} site is likely related to the bonding environment in the unit cell or the different local environment produced by the charge

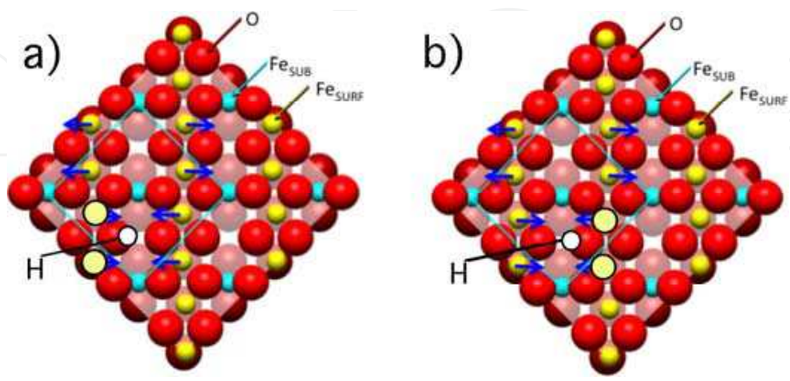

Fig. 10. Schematic model of the adsorption geometry of atomic H on the Fe_3O_4(001) surface. The H atoms preferentially bind to O atoms where the Fe(B) relax together (O_{NARROW} site) and the neighboring Fe(B) become brighter. In (b) the H has jumped to the opposite O_{NARROW}, and the Fe(B) on the opposite Fe(B) pair becomes bright. Figure adapted from Ref. 32

ordering in the subsurface layers. At 1/8 ML coverage, one O_{NARROW} site per unit cell is hydroxylated, and a (√2×√2)R45° ordering is observed amongst the adsorbates in STM [32].

When the H coverage is increased past 1/8 ML the O_{WIDE} sites begin to be occupied. Figure 11 shows an STM image in which the total coverage is approximately 1/6 ML, but locally there are some rows with slightly higher and lower occupation. In some places one can still clearly see the undulating rows of Fe(B) atoms (green arrow), but there are also rows in which long sections are affected by the H atoms. In such rows (one is indicated by the blue dashed line in figure 11) the Fe(B) atoms appear to be straight. The straightening of the Fe(B) rows with H adsorption is consistent with the observation from LEED that the saturated surface reverts to (1×1) symmetry.

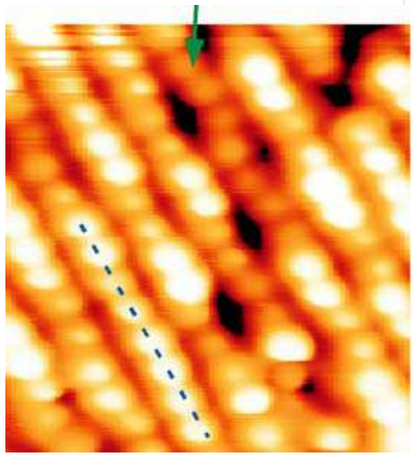

Fig. 11. STM image (4x4 nm², V_{SAMPLE}=1.2 V, I_{TUNNEL}=0.3 nA) showing the straight Fe(B) rows (blue dash line) formed following atomic H adsorption on the Fe_3O_4(001) surface. The green arrow indicates an area of reconstructed surface. Adapted from Ref. 32

The atomically resolved structural studies clearly show that atomic H causes the surface Fe rows to revert to a bulk-like arrangement. However, it is important to understand whether the surface metallization occurs because the surface is bulk-like, or if the adsorption of atomic H leads creates a surface distinct from the bulk with its own unique properties.

The method most commonly used to investigate crystal properties from a theoretical standpoint is density functional theory (DFT) [68], for which Walter Kohn was awarded the Nobel Prize for chemistry in 1998. In DFT, the ground state energy of a system is calculated through the minimization of an energy functional, which depends only on the electron density in the system. The energy functional contains terms related to the kinetic energy of the electrons, their interaction with the atomic nuclei, and their interaction with each other. The use of periodic boundary conditions allows an infinite crystal to be calculated using a small slab of atoms, typically numbering less than 100. The calculations yield the electron density and with it the optimum geometry of the system. This can be used to shed light on physics underlying phase transitions, electrical, magnetic and optical behavior. It should be noted that the accuracy of DFT relies heavily on the energy functional used, and that the electron-electron interactions represent the most difficult aspect, particularly in highly correlated systems such as Fe_3O_4. In the calculations that follow, a Hubbard "U" parameter of 5 eV was included to account for this, more details can be found in ref. 59.

Calculations relating to the H-Fe_3O_4(001) system confirm the experimentally determined adsorption site (fig. 12a), but find that the H sits slightly off the atop site at the O_{NARROW} atom, forming a hydrogen bond to the opposite O_{NARROW} atom. This explains the facile diffusion observed in the STM movies. Moreover, the calculations show that the Fe atom pair closest to the H atom relax back to bulk terminated positions and become Fe^{2+}, which explains the change in contrast observed in STM (see fig. 9). The yellow lobes in fig. 12(b) are indicative of occupied t_2g minority orbitals, and hence Fe^{2+} character. At saturation H coverage (all surface O atoms hydroxylated) all Fe atoms in the outermost 2 layers are

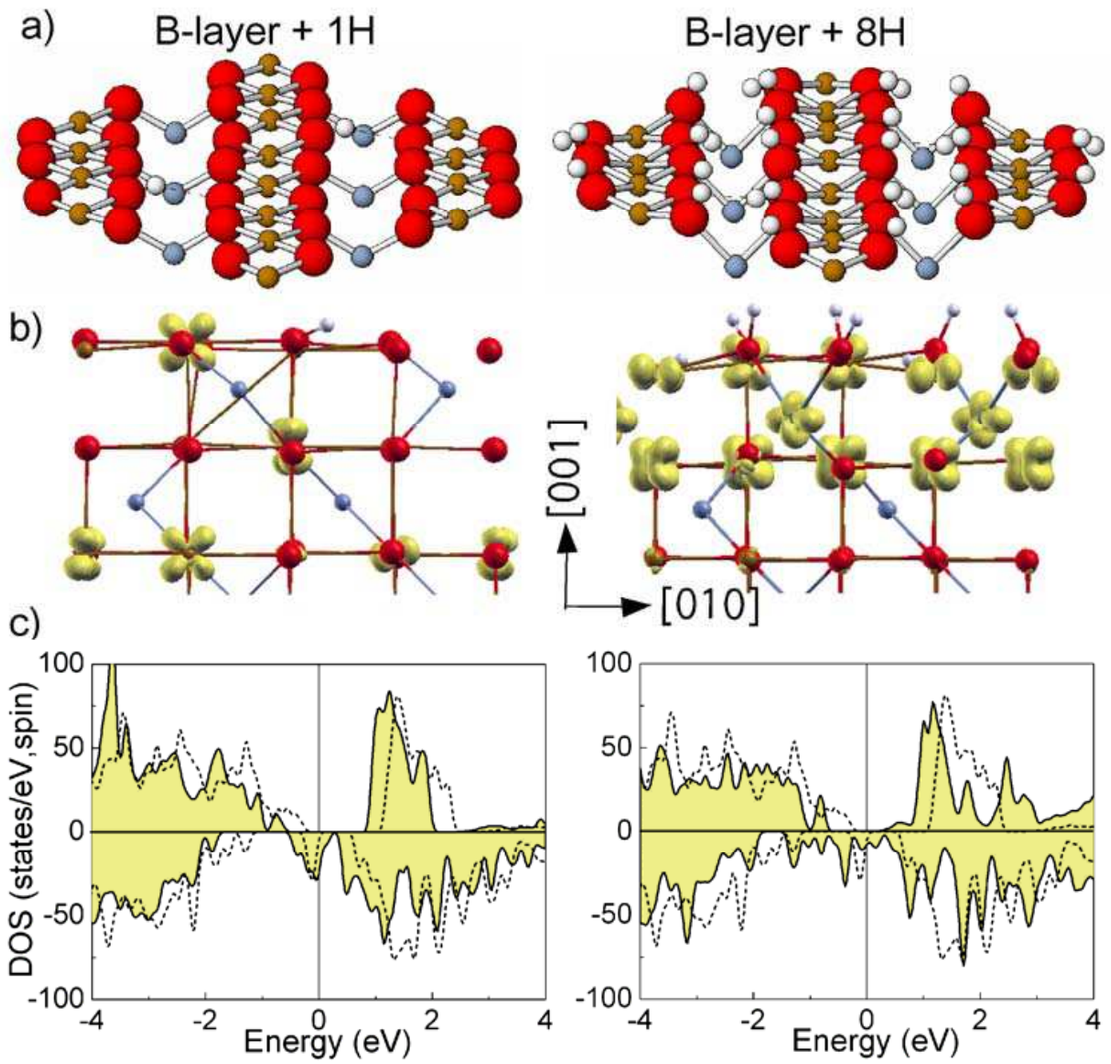

Fig. 12. Modification of an Fe_3O_4(001) surface with (left)1 and (right) 8 Hydrogen atoms per surface unit cell. O atoms are red/large, Fe(B) are gold/gray and Fe(A) are blue/light gray. (a) Adsorption geometry. (b) Side view showing the occupation of the minority t_2g orbitals at the Fe(B) sites (i.e., ions with Fe^{2+} character); electron density integrated between −1.3 eV and *E*F. (c) Total density of states (solid black line with yellow filled area) showing the characteristics of half-metallic system. For comparison the DOS of the clean surface (modified B layer; black dashed line), shows a band gap of 0.3 eV. Figure reproduced from Ref. 32

converted to Fe^{2+}, a finding consistent with the XPS results presented in figure 7b. Finally, the calculations reveal that the fully hydroxylated surface is half-metallic, that is, has only minority spin electrons present at the Fermi level, in agreement with the metastable He scattering results. Interestingly, the calculations show that a surface with 0.5 ML atomic H (not shown), i.e., with only the O_{NARROW} and O_{WIDE} sites hydoxylated, is the closest to the bulk material, and this also exhibits half-metallicity.

6. Prospective solutions

Overall, the results described here show that the adsorption of atomic H atoms leads to localized modifications of the structural and electronic properties of the Fe_3O_4(001) surface. For H coverages in excess of 0.5 ML, the surface band gap is removed and half-metallicity is restored to the surface region. These results demonstrate that the adsorption is a valid route toward tailoring the properties of Fe_3O_4 surfaces for spintronics devices. Recent work by Pratt et al. [69] has shown that a similar half-metallization of the surface occurs with the adsorption of the organic molecule benzene. In recent years the potential of organic spintronics has been championed [70-75] as organics exhibit extremely favorable spin transport properties. If the right combination of molecule-Fe_3O_4 can be found that combines high performance with ease of fabrication and low cost, it is possible that Fe_3O_4 can play an important role in spintronics devices. In the next section we demonstrate the effect of polymer and organic coatings of magnetite nanoparticles on their magnetoresistance.

7. Tunneling magnetroresistance and spin polarization in Fe_3O_4 nanoparticles with organic coatings

In principle, a high spin polarization should result in large tunneling magnetoresistance (TMR), since the latter is proportional to the spin polarization of the tunneling electrons [76-78]. Various studies have focused on the MR ratio in Fe_3O_4 of different forms including epitaxial and polycrystalline films, powders, and tunnel junctions [39,79-82]. In early reports, some groups have claimed a large MR response on breaking contact of two microscaled single crystals of magnetite [83] and thin film structure composed of a few stacked monolayers of organically encapsulated magnetite nanocrystals [84]. However, in most cases the MR ratio is much smaller than expected, especially at room temperature. In fact, it is well known that in polycrystalline specimens and powder compacts of Fe_3O_4, the surfaces or interfaces at the grain boundaries have rather different magnetic properties and reduced spin polarization than the bulk [85-88]. This is a consequence of off-stoichiometry, surface reconstruction, oxidation, defects, and bonding effects located at or close to the surfaces and interfaces. Recently, some investigations have focused on improving MR performance of Fe_3O_4 [89-93]. Hao Zeng *et al.* reported 35% MR at 60 K for ordered three-dimensional arrays of Fe_3O_4 nanoparticles with annealing in high vacuum [89]. Rybchenko *et al.* have shown enhancement in MR of bulk granular magnetite by annealing in paraffin wax [91]. Lu *et al.* found relatively large low-field MR in ultrathin Fe_3O_4 nanocrystalline films by rapid thermal annealing at 800 °C for 120 s in pure nitrogen [92]. These works have all used passive annealing process to prevent the surfaces or interfaces from oxidation. Under ordinary conditions, the surface of Fe_3O_4 is oxidized and

contains Fe^{3+}-rich oxide [94]. Combined with surface reconstruction mentioned earlier, these two factors are believed to be the main reasons for the unsuccessful attempts to observe high spin polarization in Fe_3O_4. To reveal the true spin polarization of Fe_3O_4, the reconstruction and the Fe^{3+}-rich oxide on the surface should be lifted or removed. We have selected polymers: polystyrene (PS) [90], polycarbonate (PC) [90], poly(methyl methacrylate) (PMMA), [90] fullerene (C_{60}), hexabromobenzene (C_6Br_6) [95], and polytetrafluoroethylene (C_nF_{2n+2}, also called Teflon) as a coating layer to modify the surfaces of Fe_3O_4 nanoparticles. These coatings also serve as good insulating barriers between the Fe_3O_4 nanoparticles.

To coat magnetite nanoparticles with polymer and organic compound, α-Fe_2O_3 nanoparticles and PS, PC, PMMA, Teflon, C_{60} and C_6Br_6 with various weight ratios were mixed together by first dissolving polymer/organic compound in solvents, then adding Fe_2O_3 particles and stirring, and finally evaporating the solvent. The samples were annealed at 200 °C in pure hydrogen flow, and then pressed into pellets. The pellets were again annealed at temperatures ranging from 200 to 320 °C in pure hydrogen flow, depending on the polymers/organic compounds used.

The structural analysis was done by x-ray diffraction (XRD) and transmission electron microscopy (TEM). XRD patterns indicate that there is a complete phase transformation from α-Fe_2O_3 to inverse spinel Fe_3O_4 after annealing in hydrogen. TEM images show that the Fe_3O_4 particles are generally spherical/ellipsoidal and their size is between 10-30 nm (Fig. 13(a and c)). They are dispersed in the polymer/organic matrix. Some particles are close to each other but separated by a 1-3 nm thick layer of polymer/organic compound (Fig. 13(b)), which allows the electrons to tunnel from one Fe_3O_4 nanoparticle to another, achieving intergranular tunneling of electrons in these nanocomposites.

The transport properties of the samples were measured using the four point method in a Physical Property Measurement System (PPMS) from Quantum Design. The temperature dependence of the resistance (R) follows $\ln R \propto T^{-1/2}$, and the I-V curves are nonlinear (Fig. 14(a,b), insets). These results suggest that the electron transport in the samples is via intergranular tunneling, which has been broadly accepted as exhibiting $\exp(T^{-1/2})$ behavior in the resistance [78, 96]. We have tested the $\exp(T^{-1/4})$ form expected for variable range hopping resistance and found that R could not be described by such a law. Similar behaviors are seen in other samples.

The magnetoresistance of the samples is shown in Fig. 14. The MR of the Fe_3O_4 samples coated with PC (Fig. 14(a)) is similar to the reported data on pressed Fe_3O_4 powders and polycrystalline films [81, 97-99], which have typical MR ratio of 4-7% or lower at room temperature. The Fe_3O_4 samples coated with PMMA have almost identical results to that coated with PC. On the other hand, the sample coated with PS exhibits a MR ratio of 22.8% in an applied field of 14 T at room temperature. The maximum MR of 40.9% is obtained at 110 K (Fig. 14(b)). The MR curves show rapid change in low fields but are not completely saturated in a field of 14 T. In low field region, butterfly shaped hysteresis in MR curves have been observed, and the coercivities in the MR coincide with that in the magnetization curves for both low and high temperatures measured with either a superconducting quantum interference device (SQUID) system or PPMS (Fig. 14 (c) and (d).

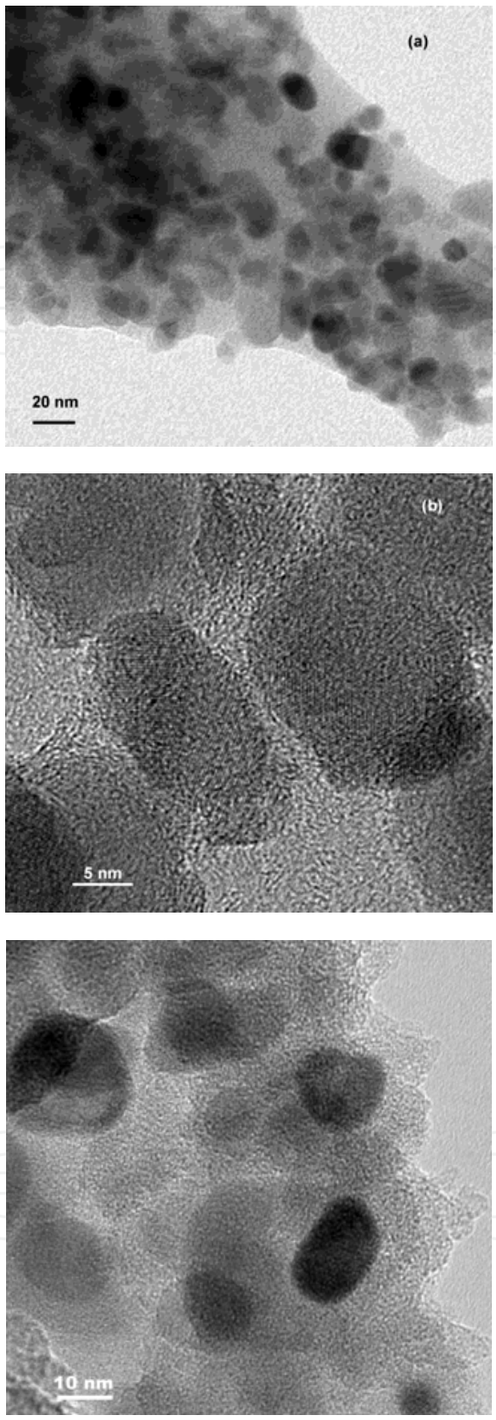

Fig. 13. (a) TEM image for the PS coated Fe_3O_4 sample indicating that spherical Fe_3O_4 nanoparticles are embedded in polymer matrix. (b) High resolution TEM image showing that the Fe_3O_4 particles are separated by a thin PS polymer layer of a few nanometers, forming tunnel barrier. (c) TEM image of a sample where Fe_3O_4 nanoparticles are dispersed in C_{60} matrix.

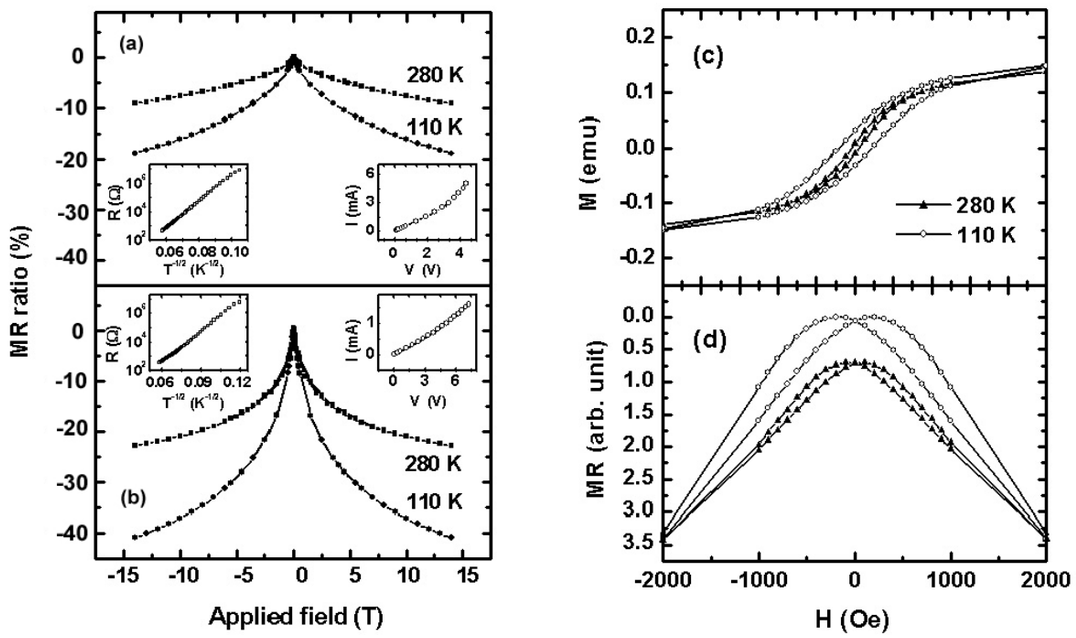

Fig. 14. MR ratio in an applied field of 14 T at 280 and 110 K for (a) PC coated Fe_3O_4 and (b) PS coated Fe_3O_4. The weight ratio of Fe_3O_4 to polymers is 1 : 1 for both. The MR ratio of PMMA coated Fe_3O_4 is similar to that of PC coated samples. (Left insets) resistance as a function of temperature: log R versus $T^{-1/2}$ curves exhibit linear relation; (Right insets) I-V curves at room temperature which have nonlinear behavior. These are consistent with the transport mechanism of intergranular tunneling. (c) Magnetic hystereses and (d) butterfly-shaped MR hyestereses in low fields for PS coated Fe_3O_4.

Several models can be used to calculate the spin polarization P from the MR data. Inoue and Maekawa have derived a simple relationship between MR and P for intergranular tunneling,[78]

$$MR = \frac{P^2 m^2}{1 + P^2 m^2} \tag{1}$$

where m is the relative magnetization of the system and m^2 = ‹cosθ›. In saturated state, m = 1, then

$$P = \sqrt{\frac{MR_S}{1 - MR_S}} \tag{2}$$

where MR_S is saturated MR ratio. A modification of the model is to consider serial connection of the grains in addition to parallel connections used in the model [100-102]. The difference between these models becomes very small when the three-dimensional nature of the network of grains is considered. This is true even for relatively high spin polarization P > 0.5. [101,102] Our composite pellet samples fall well within the 3-d regime, and Eqn. (2) was used to calculate the spin polarization. It should be mentioned that the models proposed by Slonczewski [103] and MacLaren [104] suggest that the nature of the barrier is a

factor influencing the effective spin polarization. Such an effect diminishes with increasing barrier height. The polymer/organic barriers used here are in general of very large band gap, therefore we believe the effect of the barrier on the spin polarization is small in this case. More importantly, as long as one understands that the P obtained from Eqn. (2) is the effective spin polarization, the result is valid.

The spin polarization P of Fe_3O_4 derived from the MR values according to Eqn. 2 is 83% at low temperature and 54% at room temperature. These values are much higher than the reported experimental results [105-107] and higher than a recent theoretical calculation after taking into the consideration of modified surface state [58], Fe_3O_4 indeed belongs to the category of highly spin polarized half-metals. The more than 50% value for spin polarization at room temperature is significant because this is the first time that such a high spin polarization has been observed in Fe_3O_4 at room temperature in a spin dependent transport measurement, which has both practical and scientific implications. Coulomb blockade effect is believed to be another factor that sometimes contributes to the enhancement of MR, however it occurs only at very low temperature [76,108] and should not play a significant role here. We believe these P values only set lower limits for Fe_3O_4 and the actual values of its spin polarization can be higher, especially at room temperature for the following reasons. There may exist spin independent conductance channels due to the imperfections, defects, and impurities in the barrier in our samples, which reduce the tunneling MR ratio [30]. Bulk magnons and surface magnons will reduce the MR via magnon assisted tunneling [109]. Although they may also reduce the spin polarization itself [110], theoretical studies indicate that the MR ratio will decrease more rapidly with temperature than P[111]. Even an applied field of 14 T may not be high enough to completely align the magnetic moments of the Fe_3O_4 particles of 10-30 nm in size in our samples, especially those on the surface. It should be noted that using MR data taken at 14 T to calculate P is justified because the intrinsic magnetoresistance of Fe_3O_4 is very small in such a field [81]. We have assumed that the relative magnetization m = 1 in the calculation of P using Eqn (2), but it takes a reduced value at high temperatures.

It ought to be noted that there are different ways to define spin polarization [112]. Some definitions measure the spin polarization of the density of states, while others measure the transport current density. The spin polarization obtained from our intergranular tunneling experiments is the spin polarization of the tunneling current. We argue that the spin polarization of density of states is also high for Fe_3O_4. The difference between the two definitions becomes significant when there are "heavy" (e.g., d-electrons) and "light" electrons (e.g., s-electrons) co-existing at the Fermi level, which is not the case for Fe_3O_4. For Fe_3O_4, t_{2g}(Fe) electrons form small polarons and hop among the B-sites of the inverse spinel structure in a fully spin-polarized spin-down band. Therefore, the two numbers, 54% and 83%, may also represent the approximate values for the lower limits of the spin polarization of the density of states at room temperature and 110 K, respectively.

It is necessary to study the temperature dependence of MR since Fe_3O_4 undergoes a Verwey transition, which is characterized by an increase in the resistivity by about two orders of magnitude at the transition temperature Tv ~ 120 K. This transition is associated with an order–disorder transition from a charge-ordered state of the Fe ion on the B sites at low temperature to a statistical distribution at high temperature. A sharp narrow negative MR peak is normally observed at the Verwey point in single crystal F_3O_4 [79,113]. In our

samples, the MR ratio continuously increases with decreasing temperature before the Verwey transition (Fig. 15(a)). After the transition, the MR ratio exhibits a plateau between 80 and 120 K. We cannot acquire MR data below 80 K because the resistance of the samples becomes too high to measure with our setup. According to the zero-field-cool (ZFC) and field-cool (FC) magnetization curves shown in Fig. 15(b), the Verwey transition is quite sharp and occurs in a relative narrow temperature range of 110 - 120 K in our samples. This suggests that MR observed in our samples can be used to calculate the spin polarization because it is not a part of the sharp peak ordinarily associated with the Verwey transition. The latter does not arise from the spin polarization but is a critical phenomenon at the phase transition and thus cannot be used for deriving spin polarization.

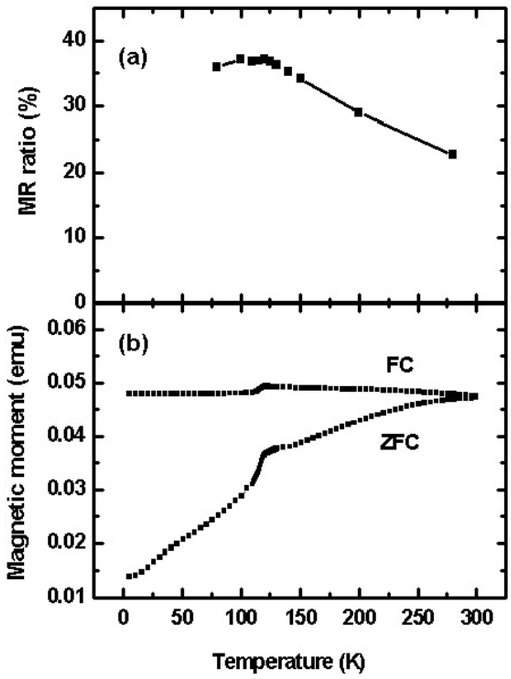

Fig. 15. (a) Temperature dependence of MR ratio in an applied field of 14 T for a PS coated sample. (b) ZFC-FC curves with an applied field H = 200 Oe, which shows sharp Vervey transiton in the range of 110 - 120 K in our samples.

The Verwey transition does not significantly change the tunneling MR and the spin polarization, consistent with reported results [105,106]. To understand the temperature dependence of MR ratio in our samples, we propose the following model. There exist two channels of the conductance. One is the intergranular spin-independent channel and the other is a spin-independent channel because of thermal excitation or inelastic hopping through localized states due to imperfections in the barrier, *etc.* Above the Verwey transition, the current of spin independent channel rapidly decreases with decreasing temperature, whereas the current of the spin dependent channel decreases relatively slowly. This results in the enhancement of tunneling MR ratio with the decrease of temperature. Below the transition, the resistance of Fe_3O_4 increases rapidly with decreasing temperature. The number of carriers available for tunneling decreases accordingly, which greatly diminishes the spin-dependent tunneling current. At the same time, the spin independent

current decreases with temperature as well. The plateau in the MR ratio below the Verwey point is the combined effect of these two channels.

XPS is one of the most powerful tools to obtain information about the electronic structure of a solid's surface. Figure 16 shows the XPS Fe 2p core-level spectra for pure Fe_3O_4 powders and PS, PMMA and PC coated Fe_3O_4 samples, which contain contributions from the top 15 layers of the surface. Different from the polymer coated Fe_3O_4 samples, the lineshape of the pure Fe_3O_4 sample exhibits shake-up satellite at a binding energy of ~719 eV and a little narrow peak of the Fe $2p_{3/2}$, which is characteristic of Fe^{3+} oxide [114,115]. This clearly demonstrates that the surface of Fe_3O_4 is Fe^{3+} oxide once it is exposed to air. The lineshapes of PS, PMMA and PC coated samples reveal the characteristics of Fe_3O_4 and there is no obvious difference among them, suggesting the coating prevented the oxygen infusion into the Fe_3O_4 particles. However, the very top layers of the surface may be different from the top 15 layers, the latter of which are probed by XPS, depending on the coating materials. Studies have indicated that the top two layers of surface are rich in Fe^{3+} compared to the top 15 layers in Fe_3O_4 films MBE-grown in ultra-high vacuum [94]. Polymer PMMA and PC contain oxygen whereas PS is oxygen free. For the PMMA and PC coated samples, it is possible to form bonding between the oxygen in polymer and Fe^{2+} ion on the surface, which will result in the presence of Fe^{3+}-rich oxide on the top one or two layers of Fe_3O_4 surface, which will greatly diminish the spin polarization as it does in pure Fe_3O_4 powders or polycrystalline film. Since PS contains no oxygen element, the Fe_3O_4 state can be preserved and the high spin polarization can survive on the surface. This greatly enhances the spin-dependent tunneling MR.

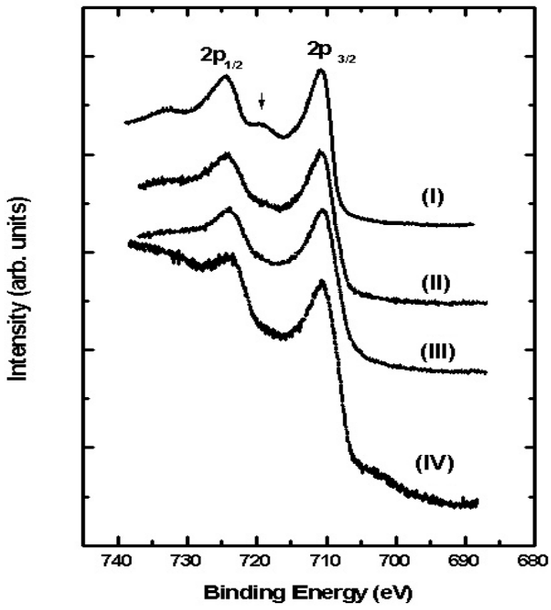

Fig. 16. Al Kα-exited Fe 2p core level photo emission spectra for (I) pure Fe_3O_4 powder sample, (II) PC coated Fe_3O_4, (III) PMMA coated Fe_3O_4 and (IV) PS coated Fe_3O_4. The arrow indicates the characteristic shake-up satellite associated with Fe(3+) ion photoemission at a binding energy of ~719 eV.

While the nanoparticle nature of the Fe_3O_4 investigated here does not allow for examination of the surface reconstruction and its potential lifting by the polymer cover layer, we have been able to study a number of other polymer/organic coatings and verify that the spin polarization of Fe_3O_4 can be preserved to a large extent when they contain no oxygen atoms.

Figure 17(a) shows the MR = $(R_H-R_0)/R_0$ of a C_{60} coated Fe_3O_4 sample annealed at 280 °C. Giant negative MR was observed at room temperature (280 K) and the MR ratio is over 11.4 % in an applied field of 5 T. The MR ratio is higher than 20 % at 150 K, however it slightly decreases to 17.6% at 75 K. These MR values are higher than reported data in pressed Fe_3O_4 powders and polycrystalline films [81,97-99], which have MR ratios typically near 4-5 % at room temperature. In our sample, C_{60} is coated on the surface of Fe_3O_4, and C_{60} is a good insulator and contains no oxygen. It may help prevent the oxidation of the surface of Fe_3O_4, which alters the half-metallic state at its surfaces.

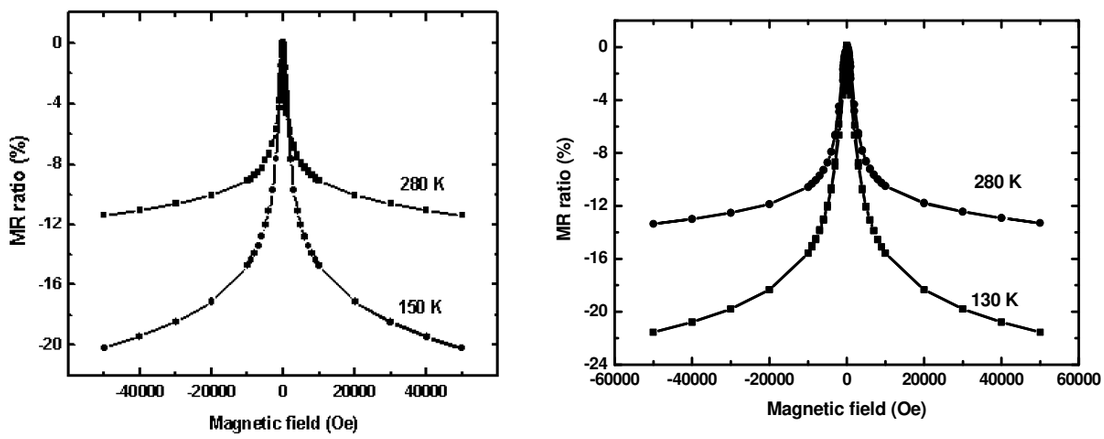

(a) (b)

Fig. 17. (a) Magneroresistance as a function of magnetic field at 150 and 280 K, respectively for a C_{60} coated Fe_3O_4 sample annealed at 280 °C. (b) That of a C_6Br_6 coated Fe_3O_4 annealed at 250 °C measured at 130 and 280 K.

Nevertheless, the MR ratio in the magnetite/fullerene nanocomposite system is relatively low compared with the results for the magnetite/polystyrene system. Polystyrene is an excellent insulator with very high resistivity (about 10^{16} Ωm). On the contrary, there exists a wide range of data for the resistivity of C_{60}, and the highest is about 10^{14} Ωm [116-118]. More importantly, many elements can be doped into C_{60}, which results in a drastic decrease of the resistivity. In our magnetite/fullerene nanocomposites, it is possible that the defects and Fe doping in C_{60} will results in an increased hopping conductance, which gives rise to an increased spin-independent current and thus reducing the MR ratio.

Figure 18 shows the room temperature MR ratio in an applied field of 5 T versus annealing temperature. There is no obvious change for the MR ratio when the annealing temperature is between 220 and 300 °C. However, for the samples annealed at 320 °C in hydrogen, the MR ratio sharply drops to about 2%. Correspondingly the resistivity also decreases rapidly and exhibits metallic behavior. X-ray diffraction pattern indicates that there is precipitation

of pure Fe in the samples. The precipitation and percolation of the iron precipitates should be responsible for the observed behaviors.

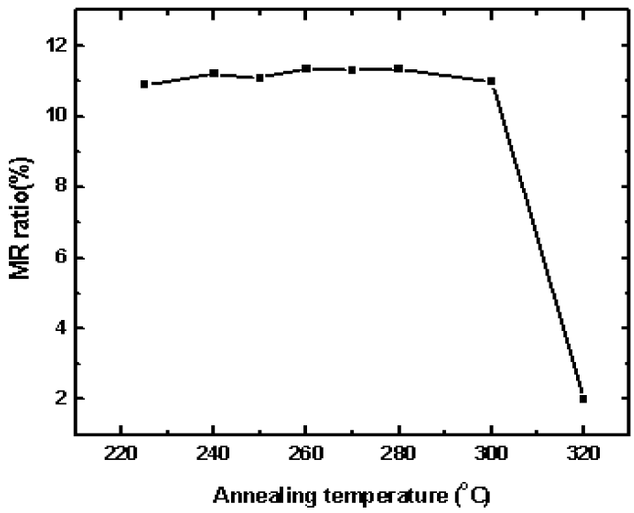

Fig. 18. Room temperature MR ratio versus annealing temperature for C_{60} coated Fe_3O_4. When the annealing temperature exceeds 300 °C, the MR ratio sharply drops to about 2% owing to the precipitation of pure Fe in the samples.

Organic compound C_6Br_6 coated Fe_3O_4 nanoparticles exhibit similar behaviors (see Fig. 17(b)). Giant negative MR was observed near room temperature (280 K) and the MR ratio is 13.4 % in an applied field of 5 T. The MR ratio is 21.5 % at 130 K, however it slightly decreases to 19.4% at 85 K.

Another oxygen-free insulating polymer, polytetrafluoroethylene (C_nF_{2n+2}), also called Teflon, was chosen as the tunnel barrier in a Fe_3O_4 intergranular tunneling experiment. A MR ratio about 16.6 % at room temperature in an applied field of 5 T was observed for a sample annealed at 320 °C in hydrogen. The temperature dependence of the resistivity exhibits characteristics of intergranular tunneling in the samples. Again, the enhancement of the MR ratio is attributed to that the Teflon can act as barrier material and, more importantly, prevent the oxidation of the surface of Fe_3O_4, which is believed to alter the half-metallic state at the surface. Our results suggest that there is high degree of spin polarization at room temperature for half metallic Fe_3O_4.

8. Magnetite nanowires

In addition to 2-dimensional epitaxial films and zero-dimensional nanaoparticles it has recently been demonstrated that fabrication of 1-dimensional nanowires, nanorods and nanotubes is possible using porous polymer or anodized alumina templates [119-121]. These structures are far less explored than the film or nanoparticulate systems, and only few reports exist on magnetoresistance of magnetite nanowires which is of the order of 7% at room temperature [122,123]. Therefore, it is believed that there is a large field for improvement of their magneto-electronic properties by functionalizing their surface, in

analogy to nanoparticle systems. The advantage of the template method is that one-dimensional magnetite structures can be fabricated in the form of regular arrays of nanopillars, which suits CPI (Current Perpendicular to the Plane) geometry of giant magnetoresistive devices. In contrast, self-assembly of nanoparticles or patterning of films is required to build spintronic nanodevices.

Below, we present a new method of fabricating magnetite nanowires by oxidation of pure Fe metallic wires [124]. Conventional mild anodized AAM with about 60 nm pore diameter and 100 nm interpore distance was prepared by two-step anodizing process. The Al substrate was removed by electrochemical process in a 1:1 mixture solution of $HClO_4$ and CH_3CH_2OH at 45 V (10 ^oC). Fe nanowires were grown in the alumina pores by electrodeposition using a solution containing 240 g/L $FeSO_4 \cdot 7H_2O$, 45 g/L H_3BO_4, and 1 g/L of Ascorbic acid with the current of -0.9 mA for several minutes using a Princeton Applied Research VMP2 instrument. In order to convert Fe metal to magnetite nanowires (while still embedded in the porous alumina) two-step oxidation process was used. First, Fe nanowires were annealed at 500^oC for 2 h in pure oxygen flow which resulted in the formation of nanowires with mixed Fe_3O_4 and Fe_2O_3 phases. Subsequently the wires were annealed at 350 ^oC in pure hydrogen flow for 2 h. This annealing reduced oxygen content and transformed the nanowires into Fe_3O_4 phase. An example of polycrystalline magnetite wires in alumina pores is presented in Fig.19. The nanowires exhibit high coercivity of 730 Oe and large saturation field of 9300 Oe. The length of the wires can be easily controlled in the range from a fraction of micrometer to several microns by adjusting electrodeposition time.

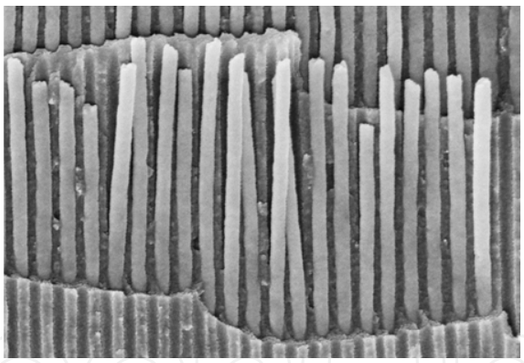

Fig. 19. Scanning electron microscopy image of Fe_3O_4 nanowires inside porous alumina template made by two step oxidation of Fe nanowires. Reproduced from ref. 124.

9. Concluding remarks

Ti-substituted magnetite ore, called loadstone, is the most common magnetic mineral on the Earth. It was also the first magnetic material discovered by humans over 2500 year ago, sparking the perpetual interest of mankind in magnetic phenomona, and resulting in first applications of magnetism in technology. Will history write another chapter for magnetite? In the era of digital compasses and Fe-Nd-B or Co-Sm permanent magnets (which eclipse the performance of magnetite by orders of magnitude), new opportunities are opening up for magnetite (in its purest form) in at least two emerging branches of nanotechnology. One of them is biomedicine, where Fe_3O_4 nanoparticles with their excellent biocompatibility are

preferred for targeted drug delivery schemes. The second avenue, spintronics, emerges from the predicted half-metallicity properties and resulting high degree of spin polarization.

Our experiments on single crystal surfaces clearly demonstrate that the presence of the most simple adsorbate, H atoms, on the Fe_3O_4 surface lifts the insulating surface reconstruction and restores half-metallic character of the surface. There remain however, many unsolved issues to be investigated, especially in reference to nanostructures which exhibit less well-defined surfaces. In particular, the role of high curvature of the surfaces in nanoparticles and nanowires is unclear. Should we expect that similar surface reconstructions occur on curved heavily stepped surfaces. To date little work has been done to assess such questions.

The recent progress in magnetoresistance of nanoparticle systems has been very encouraging. Drastic enhancements of the MR ratio clearly suggest that there is indeed a high degree of inherent spin polarization at both low and room temperatures in (theoretically) half metallic Fe_3O_4. The improvement was achieved by controlling the surface of Fe_3O_4 through surface engineering using oxygen-free insulating barriers. Based on these result, it is possible that a simple tunnel junction made of Fe_3O_4 exhibits large MR in a relatively small field, pointing toward potential application as an effective spin injector. Knowing that the surface effects can be alleviated by adsorbing appropriate adlayers, Fe_3O_4 has the potential to play an important role in spintronic devices.

10. Acknowledgments

This work was supported by grants LEQSF(2007-12)-ENH-PKSFI-PRS-04 from Louisiana Board of Regents Support Fund, EPS-1003897 through contract NSF(2010-15)-RII-UNO and National Science Foundation (DMR-0852862). GSP and UD acknowledge partial support by the Center for Atomic-Level Catalyst Design, an Energy Frontier Research Center funded by the U.S. Department of Energy, Office of Science, Office of Basic Energy Sciences under Award Number #DE-SC0001058.

11. References

[1] M.N. Baibich, J.M. Brote, A. Fert, F. NguyenVan Dau, F. Petroff, P. Etienne, G. Crauzet, A. Friederich and J. Chazelas, *Phys. Rev. Lett.* 61, 2472 (1988)
[2] G. Binasch, P. Grünberg, F. Saurenbach and W. Zinn. *Phys. Rev. B* 39, 4828 (1989)
[3] J. Barnaś, A. Fuss, R.E. Camley, P. Grunberg and W. Zinn, *Phys. Rev.*, B. 42, 811 (1990)
[4] S.S.P. Parkin, *Phys. Rev. Lett.* 71, 1641 (1993)
[5] A.E. Berkowitz, J.R. Mitchell, M.J. Carey, A.P. Young, S. Zhang, F.E. Spada, F.T. Parker, A. Hutten and G. Thomas, *Phys. Rev. Lett.* 68 (25) 37745 (1992)
[6] M. Julliere, *Phys. Lett.*, 54 A, 225-226 (1975)
[7] J. S. Moodera *et al. Phys. Rev. Lett.* 74 (16): 3273–3276 (1995)
[8] T. Miyazaki and N. Tezuka *J. Magn. Magn. Mater.* 139: L231–L234 (1995)
[9] G. A. Prinz, *Science 282*, 1660 (1998)
[10] S. Maekawa, Concepts in Spin Electronics, Oxford University Press, New York, 2006
[11] H. Kronmüller and S. Parkin, Handbook of Magnetism and Advanced Magnetic Materials, vol. 5: Spintronics and Magnetoelectronics, John Wiley and Sons Ltd., USA, 2007
[12] M. Ziese and M.J. Thornton, Spin Electronics, Springer Verlag, Germany, 2001

[13] S. Yuasa, T. Nagahama, A. Fukushima, Y. Suzuki, and K. Ando *Nat. Mat.* 3 (12): 868–871 (2004)
[14] S. S. P. Parkin et al. *Nat. Mat.* 3 (12): 862–867 (2004)
[15] M. Bibes and A. Barthélémy, *IEEE Trans. On Electron Dev.*,54, (5), 1003-1016 (2007)
[16] Y. Ji, G. J. Strijkers, F. Y. Yang, C. L. Chien, J. M. Byers, A. Anguelouch, G. Xiao, and A. Gupta, *Phys. Rev. Lett.* 86, 5585 (2001).
[17] A. Anguelouch, A. Gupta, G. Xiao, D. W. Abraham,Y. Ji, S. Ingvarsson and C.L.Chien, *Phys. Rev. B* 64, 180408 (R) (2001).
[18] L. Yuan, Y. Ovchenkov, A. Sokolov, C.-S. Yang, B. Doudin, and S. H. Liou *J. Appl. Phys.* 93, 10, 6850-6852 (2003)
[19] H. Y. Hwang and S.-W. Cheong, Science 278, 1607 ~1997!.
[20] A. Gupta, X. W. Li, and G. Xiao, *J. Appl. Phys.* 87, 6073 (2000)
[21] S. M. Watts, S. Wirth, S. von Molna´r, A. Barry, and J. M. D. Coey, *Phys. Rev*. B 61, 9621 (2000)
[22] K. Suzuki and P. M. Tedrow, *Phys. Rev. B* 58, 11597 (1998)
[23] K. Suzuki and P. M. Tedrow, *Appl. Phys. Lett.* 74, 428 (1999)
[24] S. S. Manoharan, D. Elefant, G. Reiss, and J. B. Goodenough, *Appl. Phys. Lett.* 72, 984 (1998)
[25] S. J. Liu, J. Y. Juang, K. H. Wu, T. M. Uen, Y. S. Gou, and J.-Y. Lin, *Appl. Phys. Lett.* 80, 4202 (2002)
[26] P. A. Stampe, R. J. Kennedy, S. M. Watts, and S. von Molna´r, *J. Appl. Phys.* 89, 7696 (2001)
[27] J. M. D. Coey, A. E. Berkowitz, L. Balcells, F. F. Putris, and A. Barry, *Phys. Rev. Lett.* 80, 3815 (1998)
[28] A. Sokolov, C.-S. Yang, L. Yuan, S. H. Liou, Ruihua Cheng, B. Xu, C. N. Borca, P. A. Dowben, and B. Doudin, *J. Appl. Phys.* 91, 8801 (2002)
[29] J. Dai, J. Tang, H. Xu, L. Spinu, W. Wang, K. Wang, A. Kumbhar, M. Li, and U. Diebold, *Appl. Phys. Lett.* 77, 2840 pp. 1-3(2000)
[30] J. Dai and J. Tang, *Phys. Rev., B* 63, 064410 pp.1-5 (2001)
[31] L. Dai and J. Tang, *Phys. Rev., B* 63, 054434 pp.1-4 (2001)
[32] G. S. Parkinson, *et al. Phys. Rev. B*, 125413 (125415 pp.) (2010).
[33] K. Jordan, *et al. Phys. Rev. B* 74, 085416, (2006).
[34] Z. Lodziana, *Phys. Rev. Lett* 99, 206402, (2007).
[35] J. M. D. Coey and C. L. Chien, *Mrs Bulletin* 28, 720-724 (2003).
[36] C.Park, J. G. Zhu, Y. G. Peng, D. E. Laughlin, and R. M. White, *IEEE Trans. on Magn.* 41, 2691-2693, (2005).
[37] R. Mantovan, A. Lamperti, M. Georgieva, G.Tallarida and M. Fanciulli, *J. Phys. DAppl. Phys.* 43, 11, (2010).
[38] K. S.Yoon, *et al., J. Magn. and Magn. Mater.* 285, 125-129, (2005).
[39] W. Eerenstein,T. T. M. Palstra, S. S. Saxena, and T. Hibma, *Phys. Rev. Lett* 88, (4), 247204 (2002)
[40] S. S. A. Hassan, *et al. IEEE Trans. on Magn.* 45, 4360-4363, (2009)
[41] Y. B. Xu, *et al. J. Magn. Magn. Mater.* 304, 69-74, (2006).
[42] G. Schmidt, D. Ferrand, L. W. Molenkamp, A. T. Filip, and B. J. van Wees, *Phys. Rev. B* 62, R4790-R4793, (2000).
[43] S. A. Wolf, *et al.* Spintronics: *Science* 294, 1488-1495, (2001).

[44] I. Zutic, J. Fabian, and S. Das Sarma, Spintronics: *Reviews of Modern Physics* 76, 323 410, (2004).
[45] V. Dediu, M. Murgia, F. C. Matacotta, C. Taliani, and S. Barbanera, *Sol. State Communications* 122, 181-184, (2002).
[46] R. M. Cornell, & U. Schwertmann, *The Iron Oxides: Structure, Properties, Reactions, Occurrences and Uses*. (Wiley-VCH, 2003).
[47] E. J. W. Verwey, *Nature* 144, 327, (1939).
[48] J. Garcia, & G. J. Subias, *Phys. Condens. Matter* 16, R145-R178, (2004).
[49] A. Yanase, & N. Hamada, *J. Phys. Soc. Jpn* 68, 1607, (1999).
[50] A. Yanase, & K. Siratori, *J. Phys. Soc. Jpn.* 53, 312-317, (1984).
[51] R. J.Soulen, *et al. Science* 282, 85-88, (1998).
[52] J. Osterwalder, Spin-polarized photoemission. *Magnetism: A Synchrotron Radiation Approach* 697, 95-120, (2006).
[53] M. Fonin, Y. S. Dedkov, R. Pentcheva, U. Rüdiger and G. Güntherodt, *J. Phys. Condens. Matter* 19, 315217, (2007).
[54] M. Fonin, Y. S. Dedkov, R. Pentcheva, U. Rüdiger, and G. Güntherodt, *J. Phys. Condens. Matter* 20, 142201, (2008).
[55] M. Fonin, *et al.*, *Phys. Rev. B* 72, 104436, (2005).
[56] J. G. Tobin, & et al. *J. Phys. Condens. Matter* 19, 315218, (2007).
[57] W. Weiss, and W. Ranke, *Progress in Surface Science* 70, 1-151, (2002).
[58] R. Pentcheva, *et al. Phys. Rev. Lett* 94, 126101, (2005).
[59] N. Mulakaluri, , R. Pentcheva, , M. Wieland, , W. Moritz, & M. Scheffler, *Phys. Rev. Lett* 103, 176102, (2009).
[60] G. Tarrach, D. Burgler, T.Schaub, R. Wiesendanger and H. J. Guntherodt, *Surf. Sci.* 285, 1-14, (1993).
[61] R. Wiesendanger, *et al. Science* 255, 583-586, (1992).
[62] B. Stanka, W. Hebenstreit, U. Diebold, and S. A. Chambers, *Surf. Sci.* 448, 49-63, (2000).
[63] S. F.Ceballos, *et al., Surf. Sci.* 548, 106-116, (2004).
[64] M. Kurahashi, X. Sun, & Y. Yamauchi, *Phys. Rev. B* 81, (2010).
[65] C. J. Chen, *Introduction to Scanning Tunneling Microscopy*. (Oxford University Press, 2007).
[66] U. Diebold, *Surf. Sci. Rep.* 48, 53-229, (2003).
[67] U. Diebold, J. F. Anderson, , K. O. Ng. & D. Vanderbilt, *Phys. Rev. Lett.* 77, 1322-1325, (1996).
[68] R. G. Parr, & W. Yang, *Density-Functional Theory of Atoms and Molecules*. (Oxford University Press, 1989).
[69] A. Pratt, M. Kurahashi, X.Sun, & Y. Yamauchi, *J. Phys. D-Appl. Phys.* 44, (2011).
[70] C. Barraud, *et al. Nature Physics* 6, 615-620, (2010).
[71] V. A. Dediu, , L. E. Hueso, , I. Bergenti, & C. Taliani, *Nat. Mater.* 8, 707-716, (2009).
[72] A. R. Rocha, *et al. Nat. Mater.* 4, 335-339, (2005).
[73] P. Ruden, *Nat. Mater.* 10, 8-9, (2011).
[74] S. Sanvito, & A. R. Rocha, *J. Comput. and Theoret. Nanoscience* 3, 624-642, (2006).
[75] Z. H. Xiong, D. Wu, Z. V. Vardeny, & J. Shi, *Nature* 427, 821-824, (2004)
[76] S. Mitani, S. Takahashi, K. Takanashi, K. Yakushiji, S. Maekawa, and H. Fujimori, Phys. Rev. Lett. 81, 2799 (1998).
[77] X. W. Li, A. Gupta, G. Xiao, W. Qian, and V. P. Dravid, Appl. Phys. Lett. 73, 3282 (1998).

[78] J. Inoue and S. Maekawa, Phys. Rev. B 53, R11927 (1996).
[79] V. V. Gridin, G. R. Hearne, and J. M. Honig, Phys. Rev. B 53, 15518 (1996).
[80] W. Eerenstein, T. T. M. Palstra, T. Hibma, and S. Celotto, Phys. Rev. B 66, 20110(R) (2002).
[81] J. M. D. Coey, A. E. Berkowitz, L. Balcells, F. F. Putris, and F. T. Parker, Appl. Phys. Lett. 72, 734 (1998).
[82] D. L. Peng, T. Asai, N. Nozawa, T. Hihara, and K. Sumiyama, Appl. Phys. Lett. 81, 4598 (2002).
[83] J. J. Versluijs, M. A. Bari, and J. M. D. Coey, Phys. Rev. Lett. 87, 026601 (2001).
[84] P. Poddar, T. Fried, and G. Markovich, Phys. Rev. B 65, 172405 (2002).
[85] J. M. De Teresa, A. Barhélémy, A. Fert, J. P. Contour, F. Montaigne, and P. Seneor, Science 286, 507 (1999).
[86] J. H. Park, E. Vescovo, H.-J. Kim, C. Kwon, R. Ramesh, and T. Venkatesan, Phys. Rev. Lett. 81, 1953 (1998).
[87] H. Dulli, E. W. Plummer, P. A. Dowben, J. Choi, and S. H. Liou, Appl. Phys. Lett. 77, 570 (2000).
[88] S. I. Rybchenko, Y. Fujishiro, H. Takagi, and M. Awano, Phys. Rev. B 72, 054424 (2005).
[89] Hao Zeng, C. T. Black, R. L. Sandstrom, P. M. Rice, C. B. Murray, and Shouheng Sun, Phys. Rev. B 73, 020402(R) (2006).
[90] W. Wang, M. Yu, M. Batzill, J. He, U. Diebold, and J. Tang, Phys. Rev. B 73, 134412 (2006).
[91] S. I. Rybchenko, Y. Fujishiro, H. Takagi, and M. Awano, Appl. Phys. Lett. 89, 132509 (2006).
[92] Z. L. Lu, M. X. Xu ,W. Q. Zou, S. Wang, X. C. Liu, Y. B. Lin, J. P. Xu, Z. H. Lu, J. F. Wang, L. Y. Lv, F. M. Zhang, and Y. W. Du, Appl. Phys. Lett. 91, 102508 (2007).
[93] K. Mohan Kant, K. Sethupathi, and M. S. Ramachandra Rao J. Appl. Phys. 103, 07F318 (2008).
[94] S. A. Chambers, S.Thevuthasan and S. S. Joyce, Surface Science 450, L273 (2000).
[95] W. Wang, J. He and J. Tang, *J. Appl. Phys.*, 105, (2009) 07B105.
[96] P. Sheng, B. Abeles and Y. Arie, *Phys. Rev. Lett.*, 31, 44 (1973).
[97] J. Tang , K.-Y. Wang and W. Zhou, *J. Appl. Phys.* 89, 7690(2001).
[98] H. Liu, E. Y. Jiang, H. L. Bai, R. K. Zheng, H. L. Wei, and X. X. Zhang, *Appl. Phys. Lett.* 83, 3531 (2003).
[99] D. Serrate, J. M. De Teresa, P. A. Algarabel, R. Fernández-Pacheco, J. Galibert, and M. R. Ibarra, *J. Appl. Phys.* 97, 084317 (2005).
[100] M. Ziese, Appl. Phys. Lett., 80, 2144 (2002).
[101] L. P. Zhou, S. Ju and Z. Y. Li, J. Appl. Phys., 95, 8041 (2004)
[102] S. Ju, K. W. Yu and Z. Y. Li, Phys. Rev. B, 71, 014416 (2005)].
[103] J. C. Slonczewski, Phys. Rev. B, 39, 6995 (1989).
[104] J. M. MacLaren, X. G. Zhang, and W. H. Bulter, Phys. Rev. B 56, 11827 (1997).
[105] G. Hu and Y. Suzuki, *Phys. Rev. Lett.* 89, 276601 (2002).
[106] M. Ziese, U. Köhler, A. Bollero, R. Höhne and P. Esquinazi, *Phys. Rev. B* 71, 180406(R) (2005).
[107] S. A. Morton, G. D. Waddill, S. Kim, Ivan K. Schuller, S. A. Chambers and J. G. Tobin, *Surface Science* 513, L451 (2002).
[108] T. Zhu and Y. J. Wang, *Phys. Rev. B* 60, 11918–11921 (1999).

[109] F. Guinea, *Phys. Rev. B* 58, 9212 (1998).
[110] P. A. Dowben and R. Skomski, *J. Appl. Phys.*, 95, 7453(2004).
[111] H. Itoh, T. Ohsawa, and J. Inoue, *Phys. Rev. Lett*. 84, 2501(2000).
[112] J.M.D. Coey and S. Sanvito, *J. Phy. D: Appl. Phys.* 37, 988 (2004).
[113] M. Ziese and H.J. Blythe, *J. Phys.: Condens. Matter* 12 13(2000).
[114] N.S. Mcintyre and D. G. Zetaruk, *Analytical Chemistry* 49, 1521(1977).
[115] T. Fujii, F. M. F. de Groot, G. A. Sawatzky, F. C. Voogt, T. Hibma, and K. Okada, *Phys. Rev. B* 59, 3195(1999).
[116] C.W. Chang, B.C. Regan, W. Mickelson, R.O. Ritchie and A. Zettl, Solid State Communications 128, 359–363 (2003).
[117] C. Wen, J. Li, K. Kitazawa, T. Aida, I. Honma, H. Komiyama, and K. Yamada, Appl. Phys. Lett. 61, 2162 (1992).
[118] G. B. Alers, Brage Golding, A. R. Kortan, R. C. Haddon, F. A. Theil, Science 257, 511 (1992).
[119] T. Wang, Y. Wang, F.S. Li, C.T. Xu, D. Zhou, *J. Phys.: Condens. Matter* 18 (47) 10545-10551 (2006)
[120] L. Zhang,and Y. Zhang, *J. Magn. Magn. Mater.,* 321 L15–L20 (2009)
[121] D.S. Xue, L.Y. Zhang, X.F. Xu, A.B. Gui, Appl. Phys. A–Mater. Sci.& Process 80, 439, (2004)
[122] Z.-M. Liao, Y.-D. Li, J. Xu, J.M. Zhang, K. Xia and D.-P. Yu, Nanoletters 6 (6) 1087-1091 (2007)
[123] M. Abid, J.-P. Abid, S. Jannin, S. Serrano-Guisan, I. Palaci and J.-Ph. Ansermet, J. Phys.: Condens. Matter 18 6085–6093(2006)
[124] S. Min, J.-H. Lim, L. Malkinski and J. B. Wiley, *J. Spintronics and Magnetic Nanomaterials*, 1, 52, (2012).

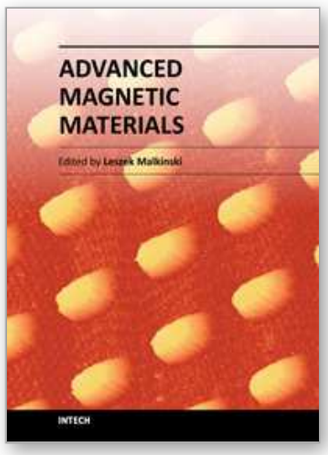

Advanced Magnetic Materials

Edited by Dr. Leszek Malkinski

ISBN 978-953-51-0637-1
Hard cover, 230 pages
Publisher InTech
Published online 24, May, 2012
Published in print edition May, 2012

This book reports on recent progress in emerging technologies, modern characterization methods, theory and applications of advanced magnetic materials. It covers broad spectrum of topics: technology and characterization of rapidly quenched nanowires for information technology; fabrication and properties of hexagonal ferrite films for microwave communication; surface reconstruction of magnetite for spintronics; synthesis of multiferroic composites for novel biomedical applications, optimization of electroplated inductors for microelectronic devices; theory of magnetism of Fe-Al alloys; and two advanced analytical approaches for modeling of magnetic materials using Everett integral and the inverse problem approach. This book is addressed to a diverse group of readers with general background in physics or materials science, but it can also benefit specialists in the field of magnetic materials.

INTECH
open science | open minds

InTech Europe
University Campus STeP Ri
Slavka Krautzeka 83/A
51000 Rijeka, Croatia
Phone: +385 (51) 770 447
Fax: +385 (51) 686 166
www.intechopen.com

InTech China
Unit 405, Office Block, Hotel Equatorial Shanghai
No.65, Yan An Road (West), Shanghai, 200040, China
中国上海市延安西路65号上海国际贵都大饭店办公楼405单元
Phone: +86-21-62489820
Fax: +86-21-62489821

IntechOpen